VOL.1, NO.3, OCTOBER 2006 ISSN 1819-6608
ARPN Journal of Engineering and Applied Sciences

www.arpnjournals.com

# PERFORMANCE ANALYSIS OF SOLAR DRIVEN HEAT ENGINE WITH INTERNAL IRREVERSIBILITIES UNDER MAXIMUM POWER AND POWER DENSITY CONDITION

A. Biswas, K. M. Pandey and R. Deb
Department of Mechanical Engineering, National Institute of Technology, Silchar, Asom, India
E-mail: agnibis@yahoo.co.in

**ABSTRACT**

Thermodynamic optimizations based on the maximum power and maximum power density criteria have been performed for a solar-driven heat engine with internal irreversibilities. In the analysis, it is assumed that the heat transfer from the hot reservoir is to be in the radiation mode and the heat transfer to the cold reservoir is to be in the convection mode. The power and power density functions have been derived, and maximizations of these functions have been performed for various design and operating parameters. The obtained results for the maximum power and power density conditions have been compared.

**Keywords:** solar, engine, power, density, finite, thermodynamics, optimization.

## 1. INTRODUCTION

Power optimization studies of heat engines using finite time thermodynamics were started by Chambadal [1] and Novikov [2] and were continued by Curzon and Ahlborn [3]. Firstly, Curzon and Ahlborn [3] studied the performance of an endoreversible Carnot heat engine at maximum power output. During the last decade, many power optimization studies for heat engines based on endoreversible and irreversible models have been performed [4]. Wu [5], Chen and Wu [6] and Chen *et al*. [7] have taken specific power output (power output per unit total heat transfer area) as the optimization criterion. The first finite time thermodynamic analysis was performed for a solar driven heat engine by Sahin [8]. He showed the optimum operating conditions for a solar-driven heat engine under maximum power output, and he also developed his model by considering the collective role of radiation and convection heat transfer from the hot reservoir [9]. Sahin *et al*. [10–12] performed optimization studies for an endoreversible Carnot heat engine and for reversible and irreversible Joule–Brayton heat engines using the power density as a new criterion. They showed that the power density analysis takes the effect of the engine size into account as related to the investment cost. Koyun [13] carried out a comparative performance analysis based on maximum power and maximum power density criteria for a solar-driven heat engine with external irreversibilities.

This paper analyzes the maximum power and the maximum power density performances for a reversible Carnot cycle with internal irreversibility of heat transfer of a solar-driven heat engine with consideration to the ratio of heat transfer area between the hot and cold reservoir which is a design parameter. Internal irreversibility factor being the other important operating parameter.

**Nomenclature**

| | |
|---|---|
| $C_H$ | hot side heat transfer coefficient |
| $C_L$ | cold side heat transfer coefficient |
| $S$ | entropy |
| $T$ | temperature |
| $\dot{W}$ | power output |
| $\dot{W}_d$ | *power output* |
| $\eta$ | efficiency |
| $x$ | $= C_H T_H^3 / C_L$ |
| $\tau$ | $= T_L / T_H$ |
| $\theta$ | $= T_X / T_H$ |

*Subscripts*

| | |
|---|---|
| C | Carnot |
| CA | Curzon–Ahlborn |
| H | heat source |
| L | heat sink |
| $\theta_{mp}$ | maximum power condition |
| $\theta_{mpd}$ | maximum power density condition |

Superscript

| | |
|---|---|
| – | dimensionless |

## 2. THE THEORETICAL MODEL

The concept of an equilibrium and reversible Carnot cycle has played an important role in the development of classical thermodynamics. The reversible Carnot cycle has been used as an upper bound for heat engines. This upper bound of performance can only be achieved through a continuum of equilibrium states required for thermodynamically reversible processes, i.e. the equilibration rate for a change of state is infinitely faster than the rate of change of state. The T –S diagram of

the considered reversible solar-driven heat engine with internal irreversibilities is shown in Figure-1.

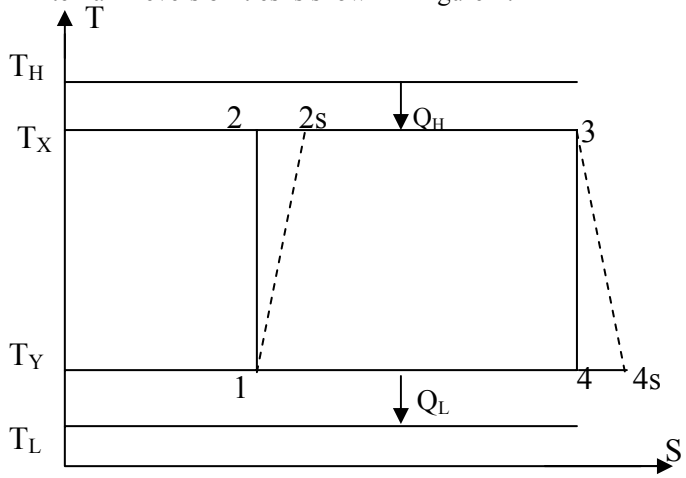


**Figure-1.** T-S diagram of a reversible solar-driven heat engine with internal irreversibility.

The heat engine operates between two extreme temperatures ($T_H$ and $T_L$). If the heat transfer from the hot reservoir is assumed to be radiation dominated then the heat flow rate $Q_H$ from the hot reservoir to the heat engine can be written as

$$\dot{Q}_H = C_H A_H (T_H{}^4 - T_X{}^4) \quad (1)$$

The heat flow rate $Q_L$ from the heat engine to the cold reservoir, assuming convection dominance, can be written as

$$\dot{Q}_L = C_L A_L (T_Y - T_L) \quad (2)$$

In Eqs. (1) and (2), $C_H$ and $C_L$ are the heat transfer coefficients of the hot and cold side heat exchangers, respectively.

From the .first law of thermodynamics, the power output of the cycle is

$$\dot{W} = \dot{Q}_H - \dot{Q}_L$$

$$= C_H A_H (T_H{}^4 - T_X{}^4) - C_L A_L (T_Y - T_L) \quad (3)$$

The thermodynamic efficiency can be written as

$$\eta = 1 - \frac{\dot{Q}_L}{\dot{Q}_H}$$

$$= 1 - \frac{C_L A_L (T_Y - T_L)}{C_H A_H (T_H{}^4 - T_X{}^4)} \quad (4)$$

Assuming an ideal gas, the maximum volume in the cycle V4 can be written as

$$V_4 = \frac{mRT_4}{P_4} \quad (5)$$

Where, m is the mass of the working .fluid and R is the ideal gas constant. In the analysis, the minimum pressure in the cycle (P4) is taken to be constant. The power density, defined as the ratio of power to the maximum volume in the cycle [14–15] then takes the form

$$\dot{W}_d = \frac{\dot{W}}{V_4} = \frac{C_H A_H (T_H{}^4 - T_X{}^4) - C_L A_L (T_Y - T_L)}{\frac{mRT_4}{P_4}} \quad (6)$$

From the second law of thermodynamics for an irreversible cycle, the change in the entropies of the working fluid for heat addition and heat removing processes yields,

$$\int \frac{\partial \dot{Q}}{T} = \frac{\dot{Q}_H}{T_X} - \frac{\dot{Q}_L}{T_Y} < 0 \quad (7)$$

One can rewrite the inequality in Eq. (7) as

$$\frac{\dot{Q}_H}{T_X} = I \frac{\dot{Q}_L}{T_Y}, \ 0 < I < 1 \quad (8)$$

With the above definition I becomes

$$I = \frac{\dot{Q}_H T_Y}{\dot{Q}_L T_X} = \frac{T_X (s_3 - s_2) T_Y}{T_Y (s_4 - s_1) T_X} = \frac{s_3 - s_2}{s_4 - s_1}$$

Substituting equation (1) and (2) in equation (8), we have

$$T_Y = \frac{T_L}{1 - \frac{C_H A_r (T_H{}^4 - T_X{}^4)}{I C_L T_X}} \quad (9)$$

Where, $A_r = A_H/A_L$= ratio of area of hot reservoir to cold reservoir

I = internal irreversibility

Substituting equation (9) in (3), (4) and (6), dimensionless power output ($\overline{W} = \frac{\dot{W}}{C_L A_L T_L}$), thermal efficiency and dimensionless power density output ($\overline{W}_d = \frac{\dot{W}_d}{C_L A_L P_4 / mR}$) can be expressed as

$$\eta = 1 - \frac{\tau}{I\theta - A_r x (1 - \theta^4)} \quad (10)$$

$$\overline{W} = \frac{A_r \eta x(1-\theta^4)}{\tau} \quad (11)$$

$$\overline{W}_d = \frac{A_r x(1-\theta^4)(I\theta - A_r x(1-\theta^4) - \tau)}{I\theta\tau} \quad (12)$$

Where, $\theta = T_X / T_H$ ;

$\tau$ = extreme temperature ratio $= T_L / T_H$ ;

x = temperature constant $= C_H T_H^3 / C_L$

To find the optimum working fluid temperature under maximum power and power density conditions, Equations (11) and (12) are differentiated with respect to θ and the resulting derivative is set to zero as

$$4A_r^3 x^2\theta^{11} + 8A_r^2 I x \theta^8 - 8A_r^3 x^2 \theta^7 + 4A_r I^2 \theta^5 - (8A_r^2 I x + 3A_r I\tau)\theta^4 + 4A_r^3 x^2 \theta^3 - A_r I\tau = 0 \quad (13)$$

$$7A^2_r x\theta^8 + 4A_r I\theta^5 - (6A_r x + 3\tau)A_r \theta^4 - A_r(\tau + A_r x) = 0 \quad (14)$$

The optimum values of θ have to satisfy Equations (11) and (12) for maximum power and power density outputs respectively. The solution of these equations can be done numerically.

## 3. RESULTS AND DISCUSSION

The variations of the normalized power (W /W max) and power density (Wd /Wd max) as functions of thermal efficiency for various extreme temperature ratios τ) are shown in Figures 2a and b, respectively (x = 0.01, $A_r$ = 2, I = 0.8). Thermal efficiency at max power ($\eta_{mp}$) and thermal efficiency at maximum power density ($\eta_{mpd}$) decrease as τ increases. Comparisons of the Carnot efficiency ($\eta_C = 1-\tau$), the Curzon–Ahlborn efficiency ($\eta_{CA} = 1 - \tau^{0.5}$), the thermal efficiency at maximum power ($\eta_{mp}$) with the thermal efficiency at maximum power density ($\eta_{mpd}$) are given in Figure-3 ( x = 0.01, $A_r$ = 2, I = 0.8). As can be seen from Figure-3, thermal efficiency at maximum power ($\eta_{mp}$) and at max. power density ($\eta_{mpd}$) vary similarly with respect to τ. Further both of these are less than the Curzon- Ahlborn efficiency when τ > 0.3.

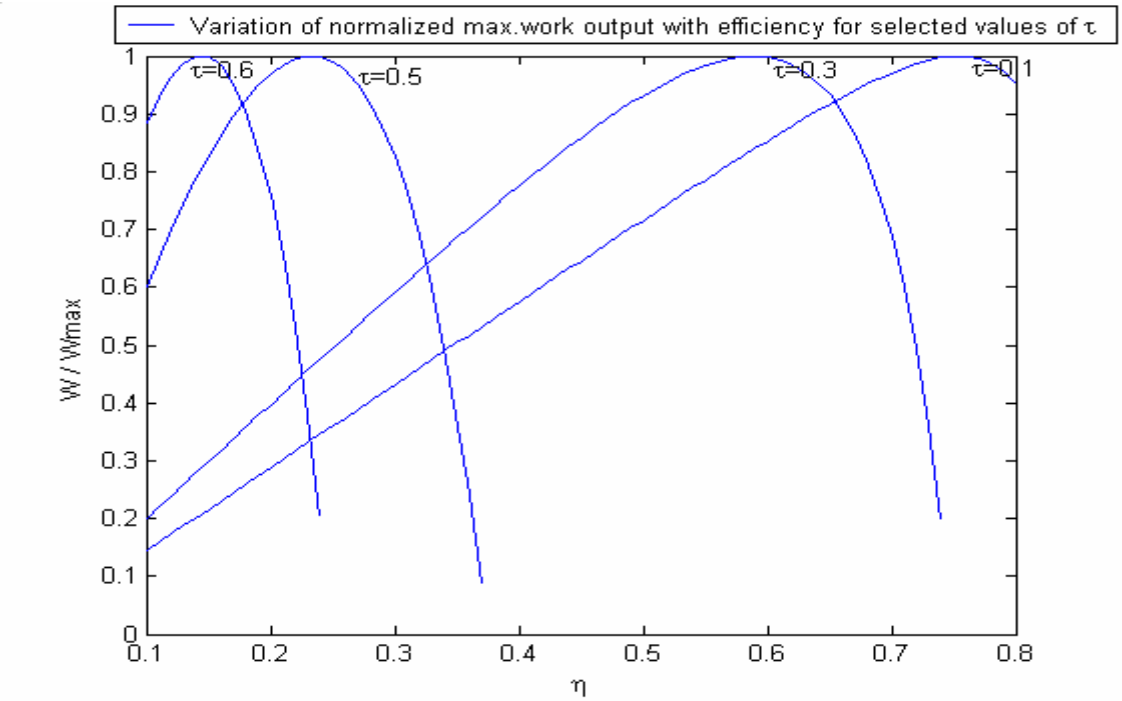


**Figure-2(a).** Variation of normalized power (work) output with thermal efficiency for different τ values ($A_r$ = 2; I = 0.8; x = 0.01).

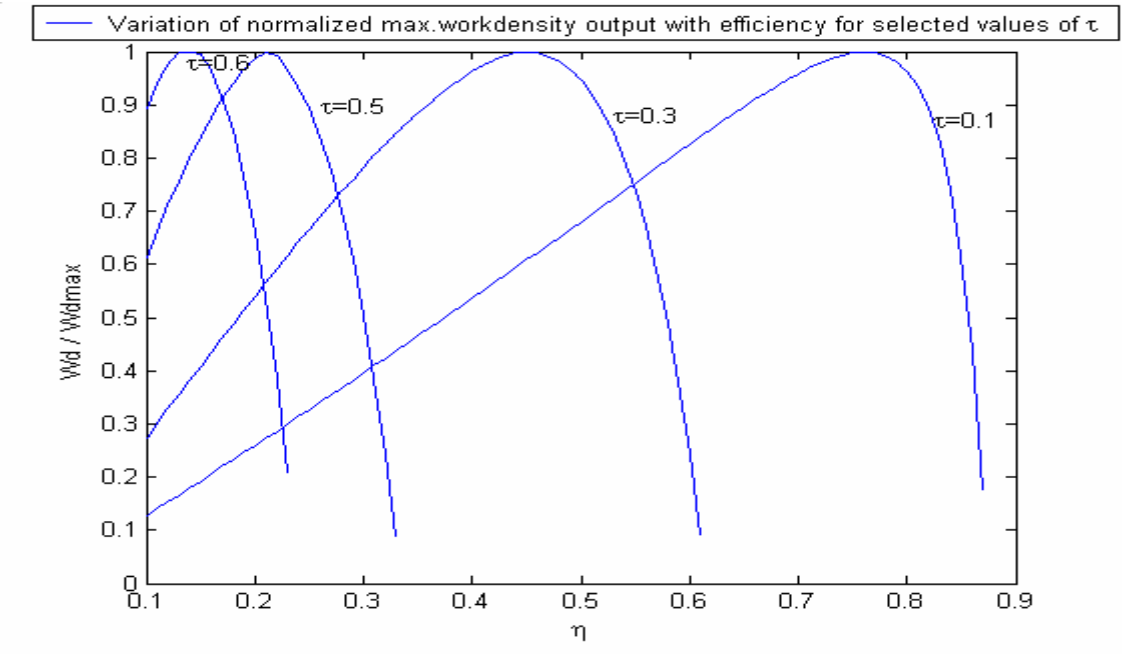


**Figure-2(b).** Variation of normalized power (work) density with thermal efficiency for different τ values ($A_r$ =2; I = 0.8; x = 0.01).

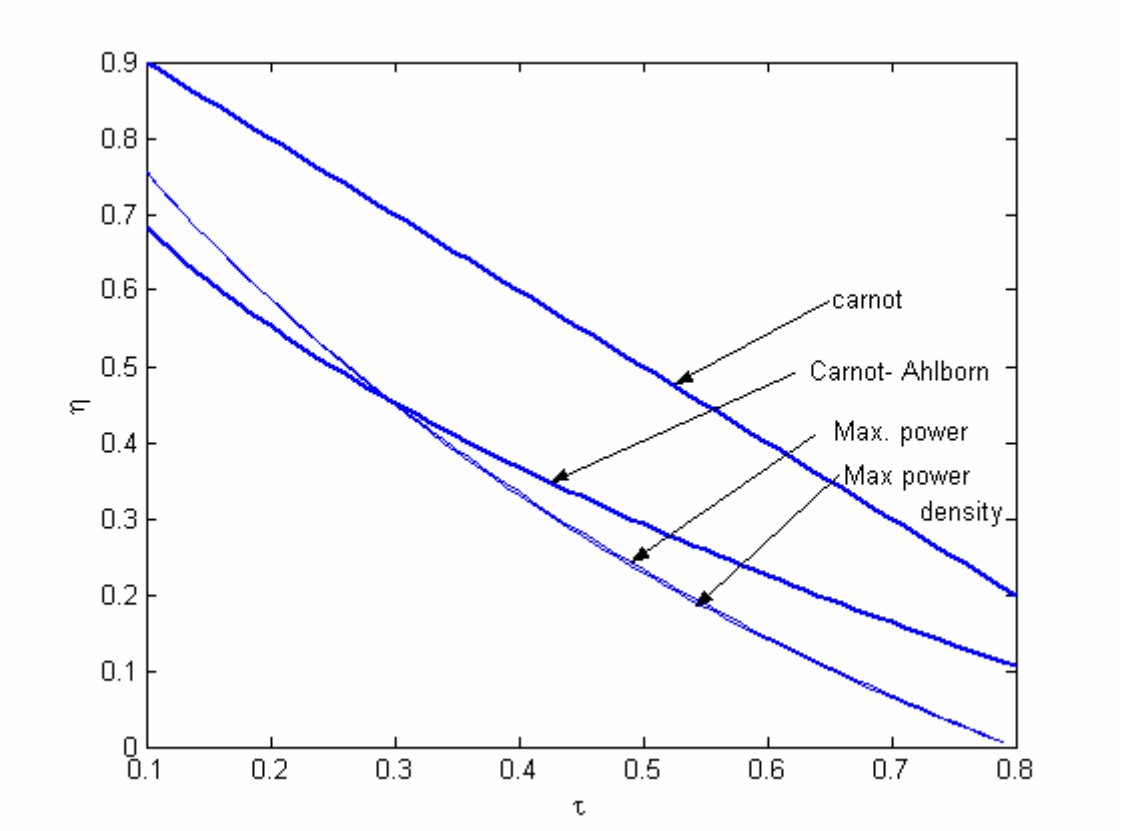


**Figure-3.** Variations of efficiency with τ ($A_r$ = 2; I = 0.8: x = 0.01).

Figures 4a and b show the variations of the normalized power (W /Wmax) and power density (Wd /Wd max) as functions of thermal efficiency for various irreversibility factors (I). Thermal efficiency at max power ($\eta_{mp}$) and thermal efficiency at maximum power density ($\eta_{mpd}$) increases as irreversibility decreases (i.e. when the values of I increases). Comparisons of the Carnot efficiency ($\eta_C = 1-\tau$), the Curzon–Ahlborn efficiency ($\eta_{CA} = 1 - \tau^{0.5}$), the thermal efficiency at maximum power ($\eta_{mp}$) and the thermal efficiency at maximum power density ($\eta_{mpd}$) are given in Fig. 5 with respect to irreversibility factor, I

(x = 0.01, $A_r$ = 2, τ = 0.3).As can be seen from the figure, the thermal efficiency at max. power density($\eta_{mpd}$) is marginally greater than that at max. power ($\eta_{mp}$) for all values of I. Also both these efficiencies are greater than the Curzon- Ahlborn efficiency when I >0.8.

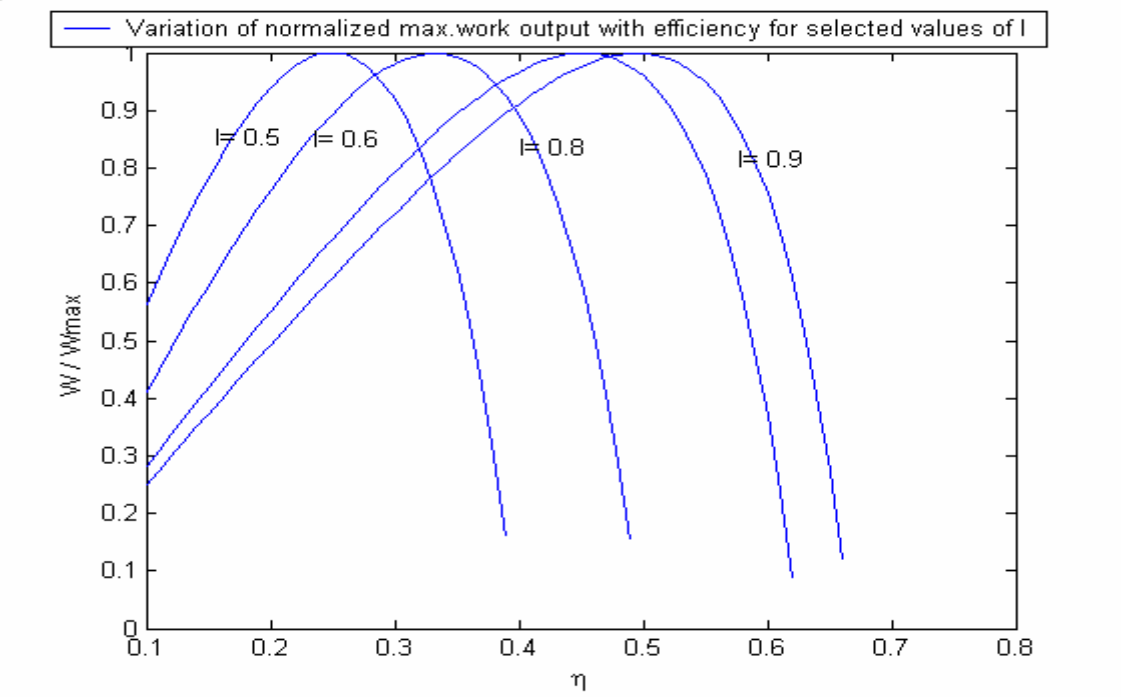


**Figure-4(a).** Variation of normalized power (work) output with thermal efficiency for different I values (Ar = 2; τ = 0.3; x = 0.01).

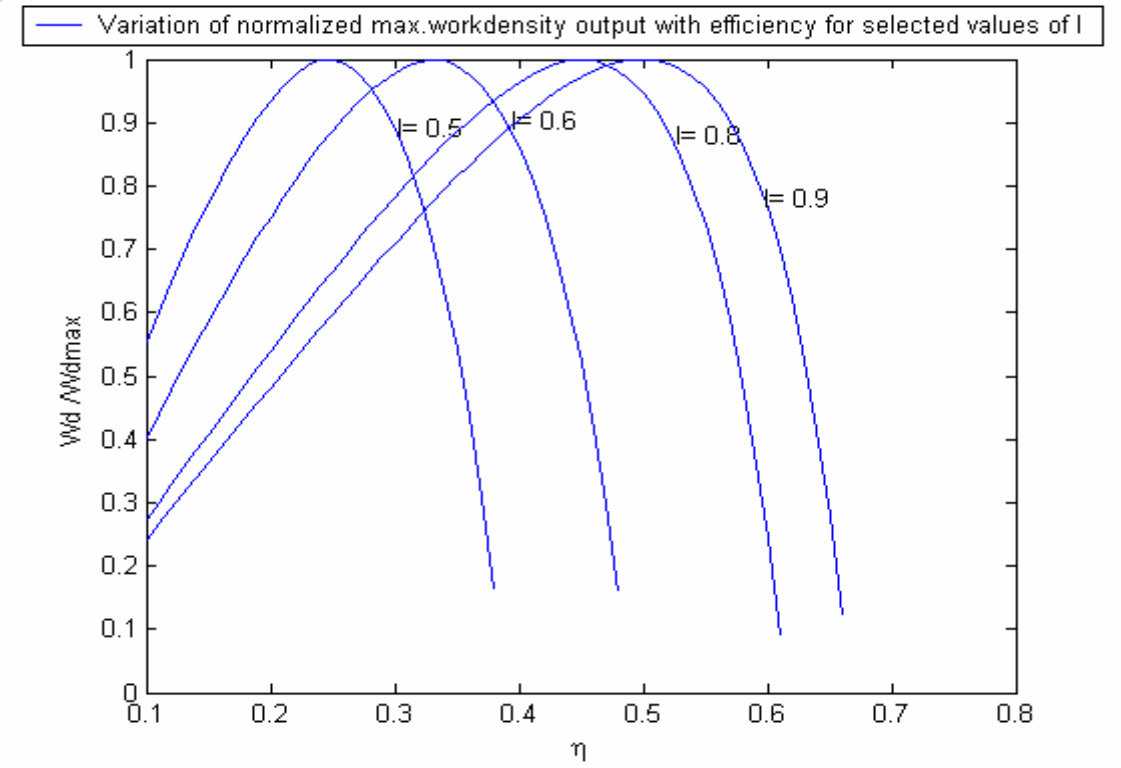


**Figure-4(b).** Variation of normalized power (work) density with thermal efficiency for different I values ($A_r$ = 2; τ = 0.3; x = 0.01).

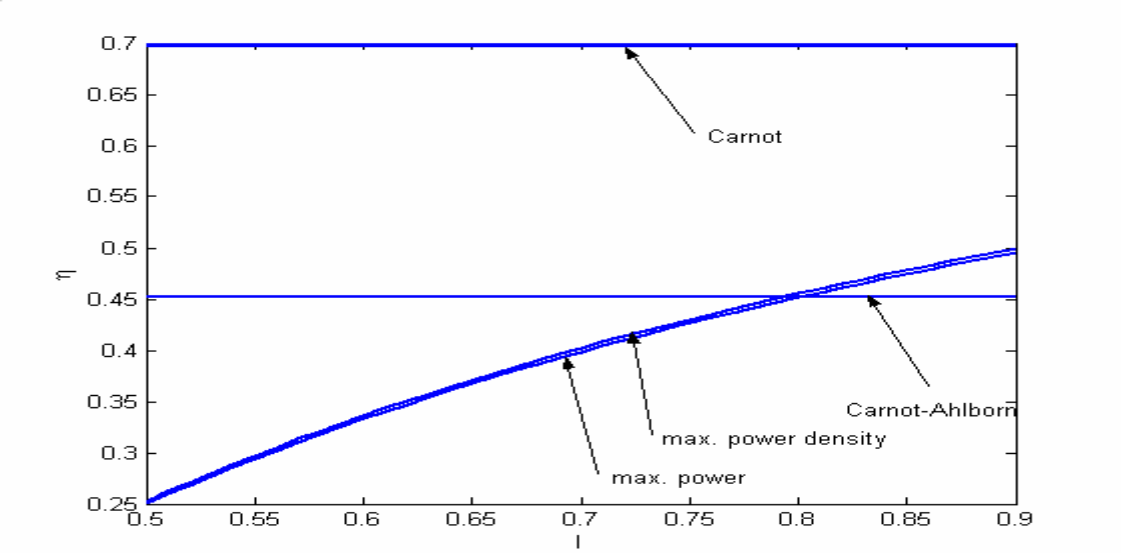


**Figure-5.** Variations of efficiency with I ($A_r = 2$; $\tau = 0.3$: x = 0.01).

The variations of the normalized power (W /W max) and power density (Wd /Wd max) as functions of thermal efficiency for various area ratios ($A_r$) are shown in Figures 6a and b, respectively (x = 0.01,$\tau$ = 0.3, I = 0.8). Thermal efficiency at max power ($\eta_{mp}$) and thermal efficiency at maximum power density ($\eta_{mpd}$) decrease as $A_r$ increases. But the decrease in efficiency at normalized power (W /W max) with respect to $A_r$ is not that great as compared to the efficiency at normalized power density (Wd /Wd max). Comparisons of the Carnot efficiency ($\eta_C = 1-\tau$), the Curzon–Ahlborn efficiency ($\eta_{CA} = 1 - \tau^{0.5}$), the thermal efficiency at maximum power ($\eta_{mp}$) with the thermal efficiency at maximum power density ($\eta_{mpd}$) are given in Figure-7 in terms of $A_r$ (x = 0.01, $\tau$ = 0.3, I = 0.8). As can be seen from Figure-7, thermal efficiency at maximum power density ($\eta_{mpd}$) is greater than efficiency at max. power ($\eta_{mp}$) for all values of $A_r$ .

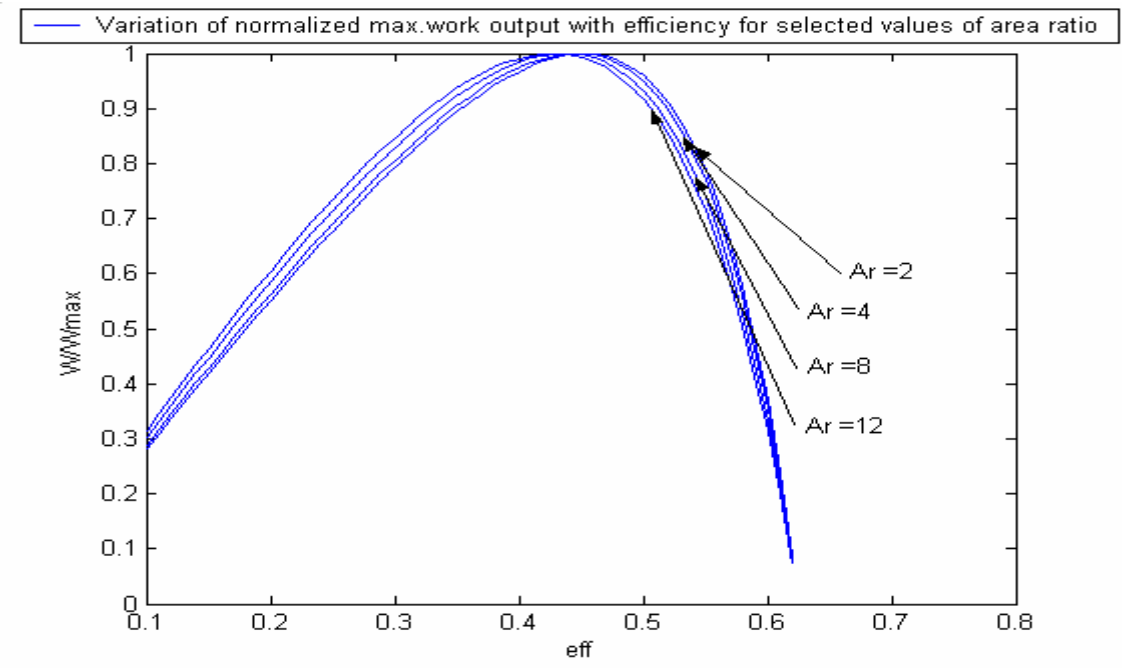


**Figure-6(a).** Variation of normalized power (work) with respect to thermal efficiency for different $A_r$ values ( I = 0.8, $\tau$ = 0.3 and x = 0.01).

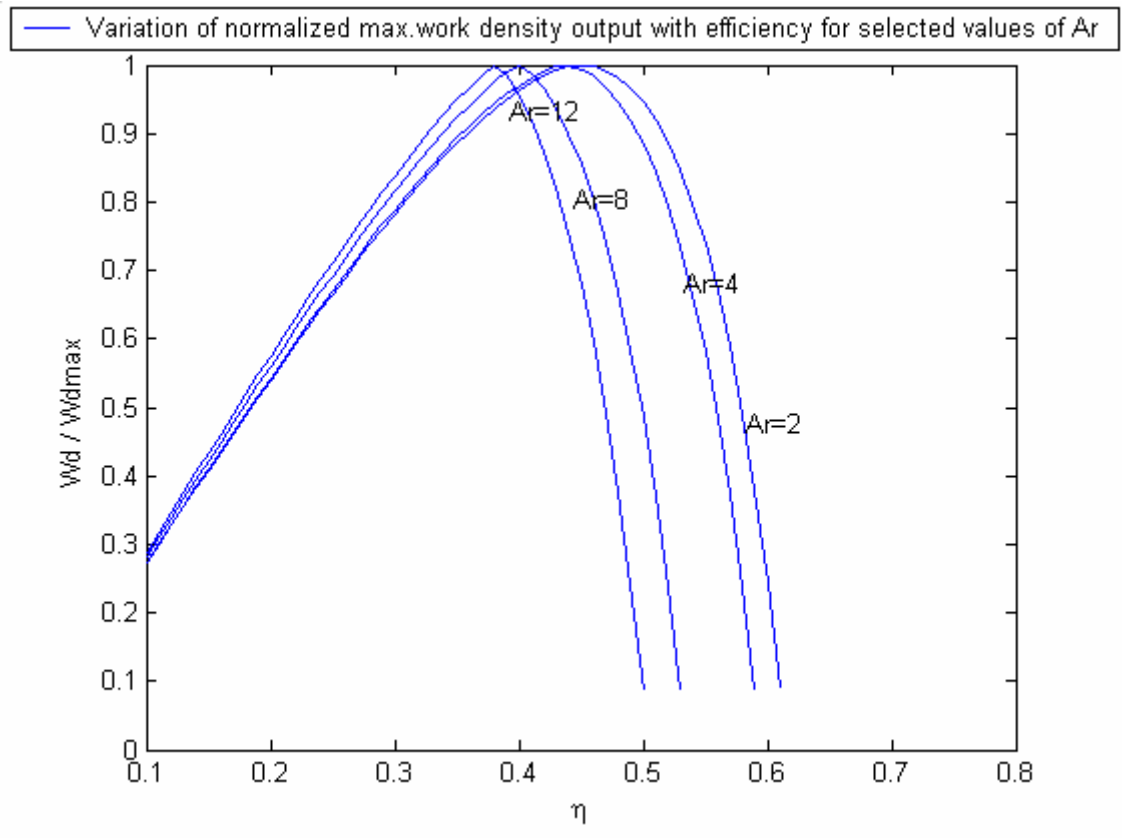


**Figure-6(b).** Variation of normalized power (work) density with respect to thermal efficiency for different $A_r$ values ( I = 0.8, $\tau$ = 0.3 and x = 0.01).

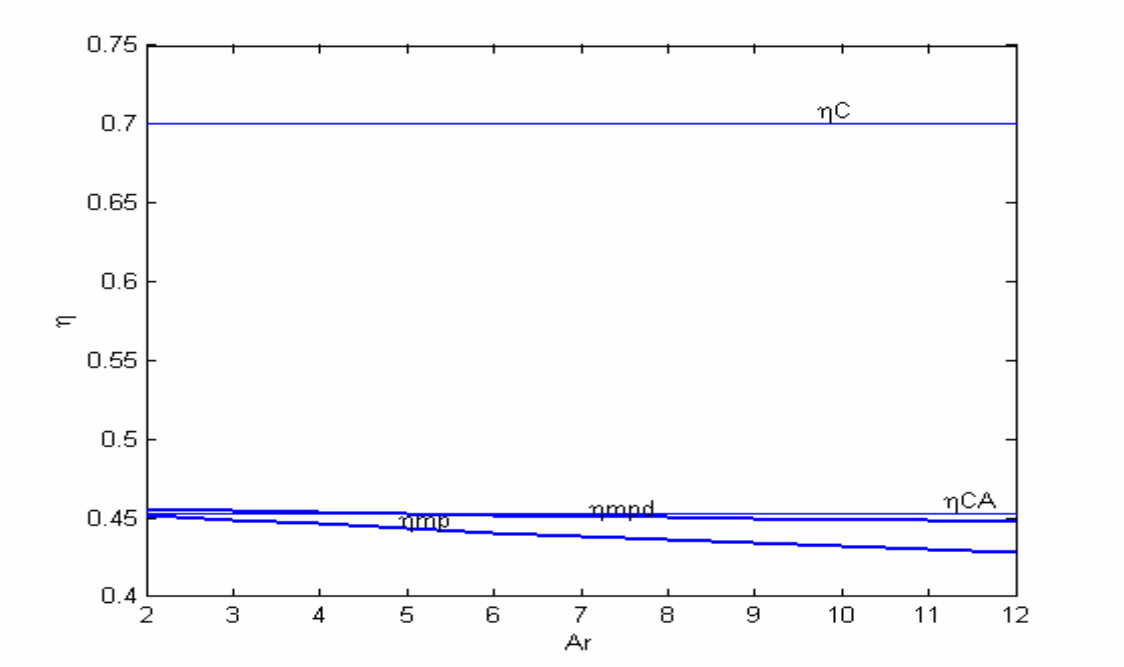


**Figure-7.** Variations of efficiency with $A_r$ (I = 0.8; $\tau$ = 0.3: x = 0.01).

Figures 8a and b show the variations of the normalized power (W /Wmax) and power density (Wd /Wd max) as functions of thermal efficiency for various temperature constant values, x ($A_r$ = 2; $\tau$ = 0.3; I = 0.8). Thermal efficiency at max power ($\eta_{mp}$) and thermal efficiency at maximum power density ($\eta_{mpd}$) increases as x decreases.

These results can be clearly seen from Figure-9. The variations of efficiency at maximum power output and efficiency at maximum power density are given with respect to x. The Carnot and Curzon–Ahlborn efficiencies are also included in Figure-9 for comparison. Since $\tau$ is taken to be constant ($\tau$ = 0.3), both $\eta_C$ and $\eta_{CA}$ are constant at 0.45 and 0.7, respectively. As can be seen from the figure, the thermal efficiency at max. power density($\eta_{mpd}$) is greater than that at max. power ($\eta_{mp}$) for all values of x and $\eta_{mpd}$ becomes equal to $\eta_{CA}$ for high value of x.. $\eta_{mpd}$ approaches $\eta_{mp}$ only for small values of x. The typical values of x for solar driven heat engines are expected to be less than 1 [13].

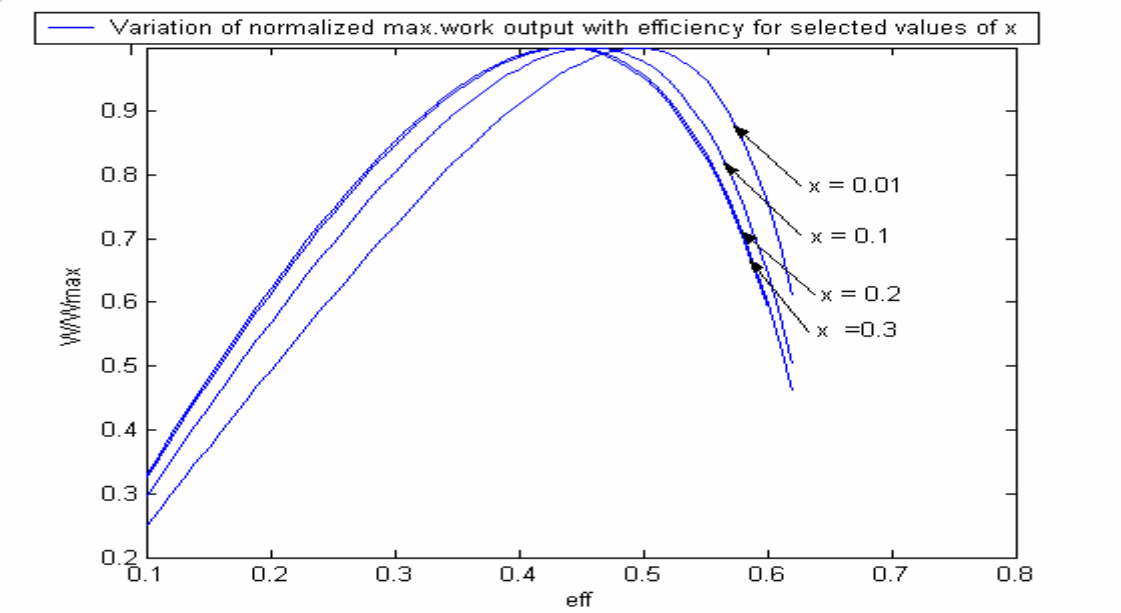


**Figure-8(a).** Variation of normalized power (work) with thermal efficiency for different x values ($A_r$ = 2; $\tau$ = 0.3; I = 0.8).

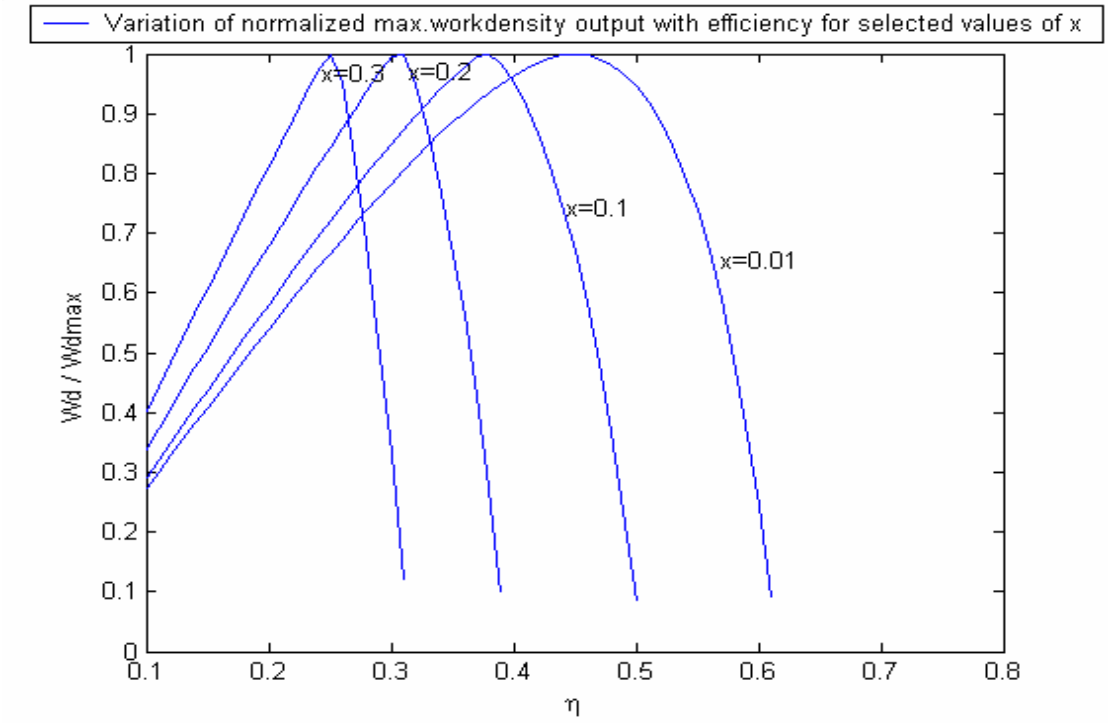


**Figure-8(b).** Variation of normalized power (work) density with thermal efficiency for different x values ($A_r$ = 2; $\tau$ = 0.3; I = 0.8).

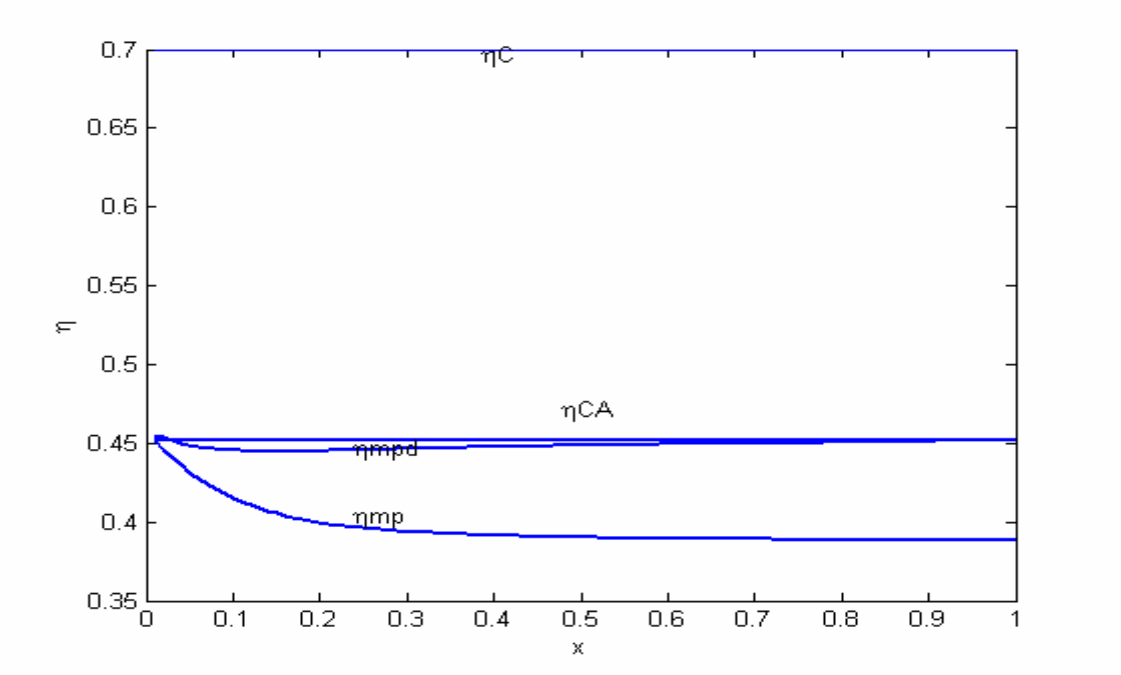


**Figure-9.** Variations of efficiency with x ($A_r = 2$; I = 0.8 ; $\tau = 0.3$).

In order to study the effects of $\tau$, x and $A_r$ on the optimum temperature values, the variation of $\theta_{mp}$ and $\theta_{mpd}$ with respect to $\tau$, x and $A_r$ are plotted in Figure-10. In these figures, $\theta_{mp}$ and $\theta_{mpd}$ correspond to the optimum $\theta$ values for the maximum power output and maximum power density conditions. As can be seen from the Figure-10(a), variations between $\theta_{mp}$ and $\theta_{mpd}$ with respect to $\tau$ is nil and both increases sharply with respect to $\tau$ and reaches 1 (x = 0.01: I = 0.8; $A_r = 2$). From Figure-10(b), it is seen that $\theta_{mpd}$ is greater than $\theta_{mp}$ for all values of x ($\tau = 0.3$: I = 0.8; $A_r = 2$). From Figure-10(c), it is observed that both $\theta_{mpd}$ and $\theta_{mp}$ increases gradually with respect to $A_r$ (x = 0.01: I = 0.8; $\tau = 0.3$) and $\theta_{mpd}$ is slightly greater than $\theta_{mp}$.

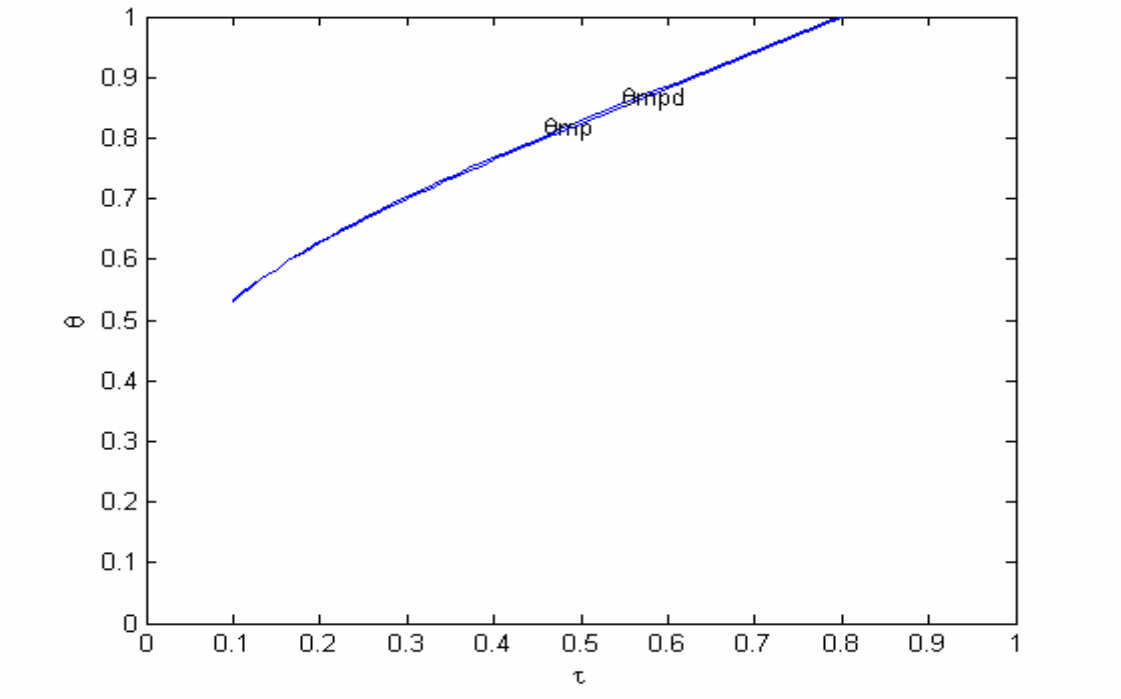


**Figure-10(a).** Variation of $\theta_{mp}$ and $\theta_{mpd}$ with respect to $\tau$ (x = 0.01: I = 0.8; $A_r = 2$).

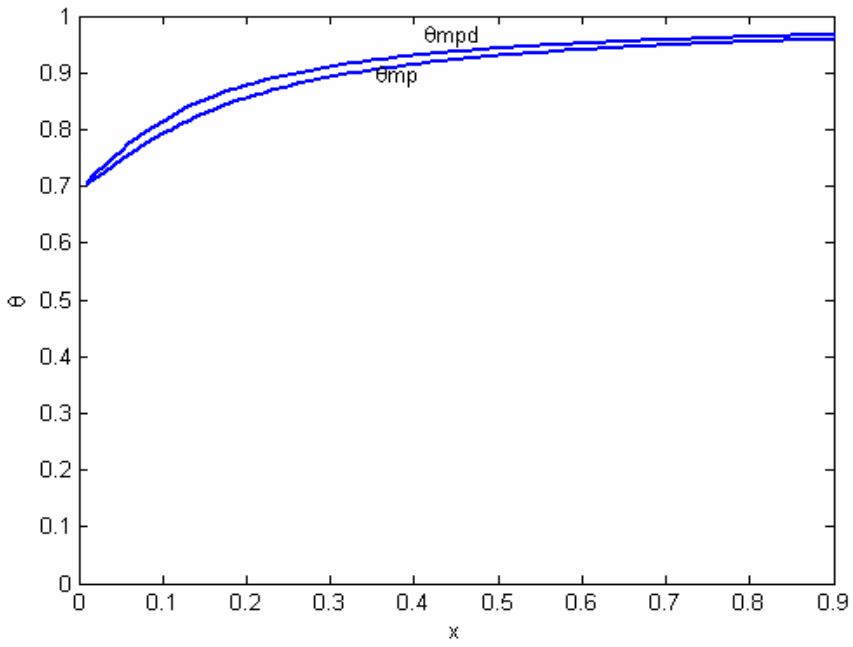


**Figure-10(b).** Variation of $\theta_{mp}$ and $\theta_{mpd}$ with respect to x ($\tau = 0.3$: I = 0.8; $A_r = 2$).

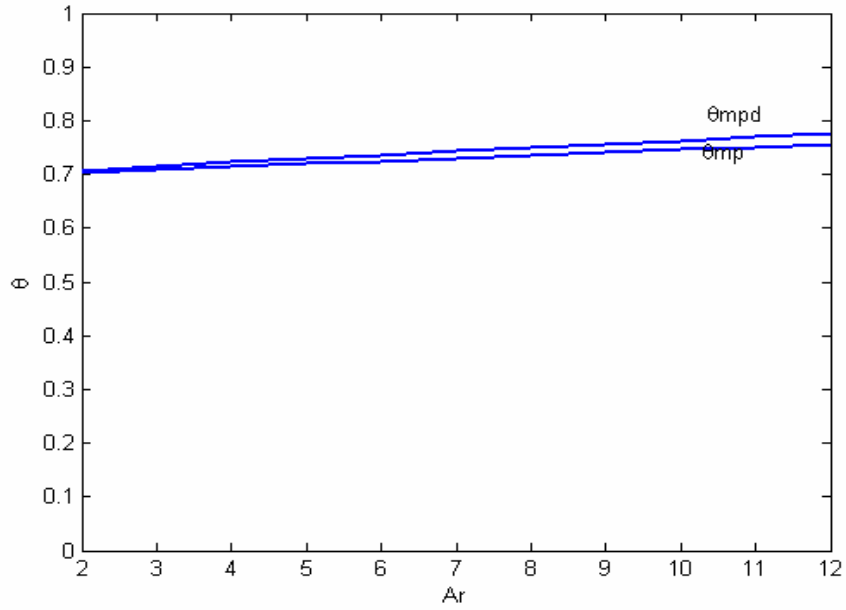


**Figure-10(c).** Variation of θmp and θmpd with respect to Ar (x = 0.01: I = 0.8; $\tau = 0.3$).

## 4. CONCLUSION

A maximum power and power density analysis of a reversible solar-driven heat engine with internal irreversibilities is performed. The obtained results are compared with published results that employ finite time thermodynamics [14]. It is shown that the efficiency at maximum power density output is bigger than the efficiency at maximum power output. It is also shown the area ratio between the reservoirs should be low & internal irreversibility should be low (i,e I >>0.7) for better performance in efficiency of the solar driven Carnot heat engine.

## REFERENCES

[1] Chambadal P. 1957. Les Centrales Nuclearies. Paris: Armond Colin. p. 41-58.

[2] Novikov II. 1957. The efficiency of atomic power stations (a review). Atom Energy. 3(11): 409.

[3] Curzon Fl, Ahlborn B. 1975. Efficiency of a Carnot engine at maximum power output. Am. J. Phys. Vol. 43: 22-24.

[4] Bejan A. 1996. Entropy generation minimization: the new thermodynamics of finite-size devices and finite-time processes. Appl Phys Rev. Vol. 79: 1191-1218.

[5] Wu C. 1991. Power optimization of an endoreversible Brayton gas turbine heat engine. Energy Convers Mgmt. Vol. 31: 561-565.

[6] Chen J, Wu C. 1996. General performance characteristics of an n-stage endoreversibe combined power cycle at maximum speci.c power output. Energy Conver. Mgmt. Vol. 37: 1401-1406.

[7] Chen J, Wu C, Kiang RL. 1996. Maximum specific power output of an irreversible radiant heat engine. Energy Conver. Mgmt. Vol. 37: 17-22.

[8] Sahin A Z. 2000. Optimum operating conditions of solar driven heat engines. Energy Conver. Mgmt. Vol. 41: 1335-1343.

[9] Sahin A Z. 2001. Finite-time thermodynamic analysis of a solar driven heat engine. Energy Int. J. Vol. 2: 122-126.

[10] Sahin B, Kodal A, Yavuz H. 1996. Maximum power density for an endoreversible Carnot heat engine. Energy. Vol. 21: 1219-1225.

[11] Sahin B, Kodal A, Yavuz H. 1995. Efficiency of Joule–Brayton engine at maximum power density. J Phys D: Appl Phys. Vol. 28:1309-1313.

[12] Sahin B, Kodal A, Yýlmaz T, Yavuz H. 1996. Maximum power density analysis of an irreversible Joule-Brayton engine. J Phys D: Appl Phys. Vol. 29: 1162-1167.

[13] Koyun A. 2004. Performance analysis of a solar driven heat engine with external irreversibilities under maximum power and power density condition. Energy Conver. Manage. Vol. 45: 1941-1947.

[14] T. Yilmaz *et al.* 2006. Optimum operating conditions of irreversible solar driven heat engines. Renewable Energy, 31. pp. 1333-1342.

BLANK PAGE